RESEARCH ARTICLE
ATMOSPHERIC PHYSICS

Earth and Planetary Physics
10: 239–250, 2026
doi: 10.26464/epp2026018

Examining charge transfer in an unusual rocket-triggered lightning flash with branched upward positive leaders

YaShun Tian[1], Xiao Li[2*], GaoPeng Lu[1*], ZiYi Wang[1], RuBin Jiang[3], Alice Nambalirwa[1], BaoYou Zhu[1], XiuShu Qie[3,4], and YiJun Zhang[5,6]

[1]School of Earth and Space Sciences, University of Science and Technology of China, Hefei 230026, China;

[2]State Key Laboratory of Chemistry for NBC Hazards Protection, Beijing 102205, China;

[3]Key Laboratory for Middle Atmosphere and Global Environment Observation (LAGEO), Institute of Atmospheric Physics, Chinese Academy of Sciences, Beijing 100029, China;

[4]University of Chinese Academy Sciences, Beijing 101408, China;

[5]State Key Laboratory of Severe Weather, Chinese Academy of Meteorological Sciences, Beijing 100081, China;

[6]Department of Atmospheric and Oceanic Sciences, Institute of Atmospheric Sciences, Fudan University, Shanghai 200438, China

Key Points:

- We examined charge transfer in an unusual rocket-triggered lightning flash and its in-cloud morphology that featured a branched upward positive leader.
- The *M*-component with huge current was formed by the connection of the dart leader with a long in-cloud channel and the main active channel.
- The branched negative leader caused the reversal of current polarity by depositing charge to ground from the positive cloud region.

Citation: Tian, Y. S., Li, X., Lu, G. P., Wang, Z. Y., Jiang, R. B., Nambalirwa, A., Zhu, B. Y., Qie, X. S., and Zhang Y. J. (2026). Examining charge transfer in an unusual rocket-triggered lightning flash with branched upward positive leaders. *Earth Planet. Phys.*, *10*(2), 239–250. http://doi.org/10.26464/epp2026018

Abstract: We have examined an unusual rocket-triggered lightning flash during the summer campaign of the SHAndong Triggered Lightning Experiment (SHATLE) in 2018. High-speed video camera observations and three-dimensional (3D) lightning mapping show that the upward positive leader split into two branched channels (referred to as branch A & branch B, respectively) at a height of about 370 m, and then progressed into different charge regions of the thundercloud. Branch A initially developed upward before turning northwest from the trigger point; ten pronounced intermittent negative leaders were observed propagating downward along this branch channel, causing strong current pulses. Branch B propagated obliquely upward towards the northeast before continuing northward to a region of weak radar echo at 3 km altitude, resulting in a large-scale charge transfer of approximately −250 C (C = Coulomb) and generating a sustained, strong current exceeding 2 kA. Furthermore, downward dart leaders propagating along branch A connected to the active channel of branch B at the bifurcation point. This connection generated a surge of large current pulses (*M*-components) superimposed on the continuing current. Evidence from 3D lightning mapping and concurrent channel-base current measurements suggests that the 10th negative dart leader split during its downward propagation, with one branch propagating to ground, while the other entered into a positive charge reservoir. This initiated a positive charge transfer to ground via the existing channel, ultimately triggering the final stroke which exhibited a bi-polarity current pulse.

Keywords: lightning morphology; charge transfer; *M*-component; three-dimensional (3D) lightning mapping; rocket triggered lightning

Plain Language Summary

Cloud-to-ground (CG) lightning transfers varying amounts of electric charge from thundercloud to ground by developing in-cloud conductive channel networks of differing complexity. The ways that lightning channels evolve inside parent thunderstorms have been identified as worthy of study because channel patterns might significantly affect the magnitude of charge transfers to ground. We have examined in detail an unusual rocket-triggered lightning flash of negative polarity with visible extensive branching to study the behavior of charge transfer to ground. Charge transfer along each channel was estimated based on the channel-base current. Flash morphology was imaged using the time-of-arrival (TOA) method applied to data from a low-frequency magnetic field lightning mapping array (LFM-LMS). Positions of charge regions in the thundercloud were determined; current moments

First author: Y. S. Tian, tys2018@mail.ustc.edu.cn
Correspondence to: X. Li, hxzzlx@163.com
G. P. Lu, gaopenglu@gmail.com
Received 20 JUL 2025; Accepted 11 OCT 2025.
First Published online 24 DEC 2025.
©2025 by Earth and Planetary Physics.

were calculated based on those source locations and channel-base currents. Our study contributes to comprehending the connection between in-cloud lightning morphology and the charge transfer of relevant processes, such as the continuing current, *M*-component, and CG strokes of the triggered lightning.

1. Introduction

Lightning is a spontaneous momentary high-current discharging process involving charge transfers on a variety of spatial and temporal scales between oppositely charged cloud regions in parent thunderstorms, or from cloud to ground in the form of cloud-to-ground (CG) lightning (Rakov and Uman, 2003). Its three-dimensional (3D) morphology, duration, peak current, and the amount of charge transfer are key parameters that characterize the scale and intensity of a specific lightning flash. Most previous efforts have treated the charge transfer as the feature most relevant to practical concerns on lightning safety and its effects in near-Earth space (e.g., Wang D et al., 1999; Lu GP et al., 2009, 2012). In particular, the CG stroke and following process can produce high peak current and large charge transfer, causing transient luminous events (TLEs) in the mesosphere, such as haloes and red sprites (Pasko et al., 1997; Lu GP et al., 2013, 2016a; Ren H et al., 2019, 2021).

Lightning location technology, based on multi-band lightning pulse detection, provides a proven technique for characterizing the 3D spatial morphology of lightning. Many location networks, operating at different frequencies, have achieved this goal, such as the Lightning Mapping Array (LMA) developed by New Mexico Tech that operates in the very high-frequency (VHF) band to provide 3D images of intra-cloud (IC) or CG lightning (Rison et al., 1999; Thomas et al., 2004). In recent years, 3D lightning imaging techniques have developed rapidly, some based on measurements of fast electric field (*E*-field) change (Bitzer et al., 2013; Karunarathne et al., 2013; Yoshida et al., 2014; Shi DD et al., 2017; Wu T et al., 2018; Yuan SF et al., 2020), others on magnetic pulses (Lyu F et al., 2014, 2016) in the low-frequency (LF) band.

To quantify charge transfer associated with cloud-to-ground (CG) strokes, Krehbiel et al. (1979) developed a method utilizing electric field change (ΔE) measurements from multiple slow antennas. Subsequently, Maggio et al. (2009) employed point-charge or distributed-charge models to infer both the location of lightning discharges and the magnitude of transferred charge. Meanwhile, lightning mapping has been coordinated with measurements of lightning-induced *E*-field change (Sonnenfeld et al., 2006; Lu GP et al., 2011), or remote sensing of lightning current (Lu GP et al., 2012, 2013), to study charge transfer in lightning. The magnitude of charge transfer is usually evaluated as the *charge moment change* (CMC), which is defined as the product of total charge transfer from cloud to ground and its original height above the ground (Cummer and Lyons, 2004).

In classical rocket-triggered lightning, the discharge commences with an upward-propagating positive leader, typically followed by a quasi-steady initial continuous current (ICC) with a duration ranging from tens to hundreds of milliseconds and an amplitude of approximately 100 A; thereafter, one or more subsequent CG strokes may occur with high peak currents and intense electromagnetic radiation (e.g., Fisher et al., 1993; Qie XS et al., 2010). Rocket-triggered lightning experiments, featuring synergistic measurements of channel-base current, high-speed optical imaging, electric field changes, magnetic fields, and very high frequency (VHF) radiation, provide an effective means for investigating lightning charge transfers, associated physical effects, and their meteorological conditions (Edens et al., 2012; Qie XS et al., 2014; Fan YF et al., 2020). Thus, the study of rocket-triggered lightning facilitates investigation of the spatial development of natural lightning and its charge transfer, which is important to understand the influence of lightning morphology on the magnitude of charge transfer and associated physical and chemical effects.

In this study, comprehensive measurements and analysis were conducted with respect to an exceptionally rare rocket-triggered lightning flash captured during the summer of 2018. High-speed optical recordings reveal that the upward leader of this triggered lightning split into two channels: one channel (branch B) carried a high-intensity continuing current, while the other channel (branch A) induced ten recoil negative breakdown that caused intense *M*-components or subsequent strokes. Our preliminary goal was to clarify why one channel always remained luminous with persistent charge transfer to ground, while the other channel was lit and then extinguished several times in a repetitive manner accompanied by *M*-components or CG strokes.

We reconstructed the 3D structure of lightning with a network of LF magnetic field detection (Li X et al., 2023), and calculated the charge transfer from the thundercloud to ground based on the measurement of channel-base current. In addition, we examined the source of charge transfer by matching it to radar observation of reflectivity. Our work may shed light on the connection between lightning morphology and the characteristics of charge transfer.

2. Measurements and Data

The unusual triggered lightning of interest was observed at 23:38:25 UTC on 7 August 2018 during the SHAndong Triggered Lightning Experiment (SHATLE) in Zhanhua, Shandong Province (Qie XS et al., 2010). In the following discussion, this event was referred to as Tr_201807 (namely the 7th triggered lightning in 2018 at SHATLE). A Phantom V711 high-speed video camera was deployed at the main observation site, 970 m from the triggering site, to record the evolution of lightning channels at 14,000 fps (with frame interval of 71.43 μs); the spatial resolution is 1024 × 512 pixels. *B*-field and d*E*/d*t* measurements were also implemented at the main observation site (Li X et al., 2019). The channel-base current, measured with a 5-mΩ shunt (with bandwidth of 3.2 MHz), was digitized and recorded with an oscilloscope at a sampling rate of 20 MHz (Jiang RB et al., 2013).

A lightning mapping network of seven LF magnetic field recording stations (referred to as LFM-LMS) was operated to locate the electromagnetic pulses radiated by lightning discharges (e.g. Lyu F et al., 2014; Li X et al., 2023). The LF stations were installed around the triggering site typically within a range of 10 km (Ma Z et al., 2021). At each station, the magnetic field signal was detected by

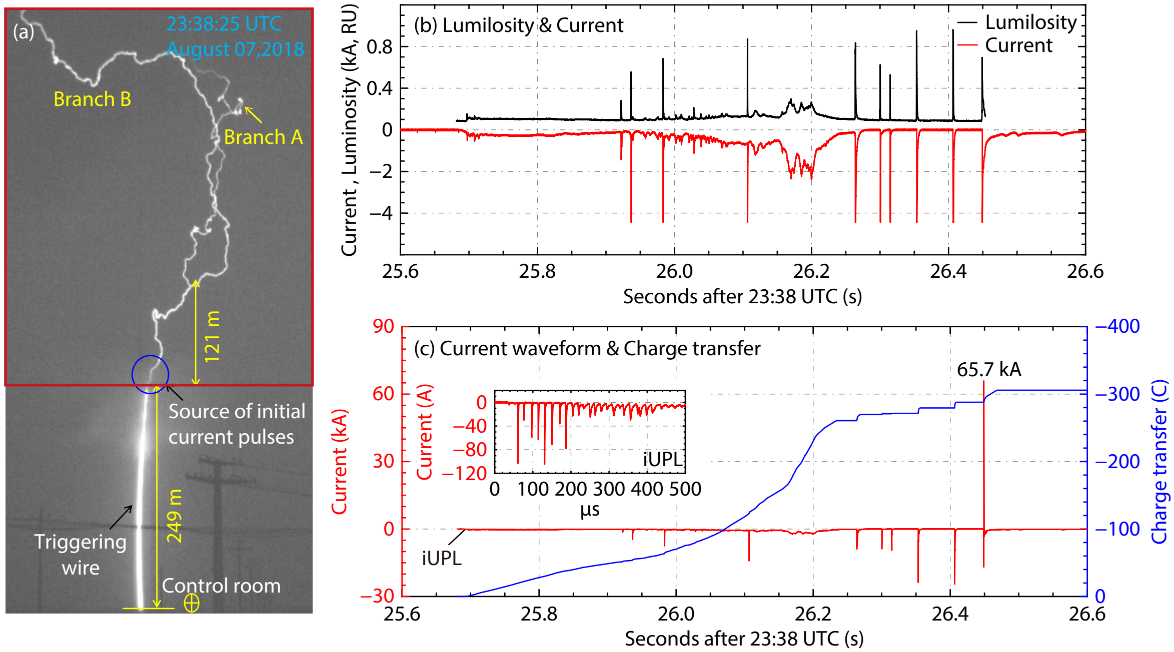

Figure 1. (a) Snapshot of the triggered lightning flash (Tr_201807) examined in this paper (the area outlined by the red rectangle corresponds to the region used for the brightness integration); (b) Current waveform measured with the high-gain setting and luminosity curve of the flash; (c) Current waveform measured with the low-gain setting and corresponding charge transfer. The inset in panel (c) shows the impulsive and ripple pulses of the initial upward positive leader (e.g., Lu GP et al., 2016b; Fan YF et al., 2018).

two orthogonal induction coils and recorded continuously at a sampling rate of 1 MHz; the 3-dB bandwidth of magnetic field sensing is 30–500 kHz. The recordings of high-speed images, channel-base current, and LF magnetic signals were synchronized by GPS receivers with time accuracy better than 50 ns. In addition, an S-band meteorological radar located in Binzhou, Shandong Province, approximately 55 km from the SHATLE, provided radar scans of precipitation reflectivity during the entire thunderstorm.

3. Analyses and Results

Figure 1 shows images of the rocket-triggered lightning, along with the temporal variations of optical intensity, channel base current, and charge transfer. We calculated relative luminosity by integrating brightness, in each frame of the high-speed video, within a rectangular region covering the entire discharge channel. Based on the high-speed video imagery (Figure 1a) and current waveforms (Figure 1b), our analysis reveals that the lightning commenced with a series of initial upward leader pulses (see the inset of Figure 1c), subsequently branching into two upward leaders (labeled as branch A and branch B, respectively in Figure 1a) that meandered upward into the thundercloud.

Visual inspection of the video imagery revealed that ten downward negative leaders propagated along branch A from the bottom of thundercloud to the bifurcation point, transferred charge to ground, and initiated *M*-components or CG strokes (Wang D et al., 1999). Meanwhile, branch B glowed continuously and transferred charge steadily to ground until the lightning channel faded from view in the camera's field of vision. Ten prominent pulses shown in the relative luminosity curve (black line in Figure 1b) correspond to the processes of downward leader and *M*-components (the first five pulses denoted as P#1–5) or CG strokes (the next five pulses denoted as P#6–10) in branch A, which can also be identified in the d*E*/d*t* waveform (magenta line in Figure 2b) and magnetic field signal (royal-blue line in Figure 2b). The peak current of the stroke reached −24.53 kA (+65.7 kA). This lightning flash lasted approximately 0.98 s, commencing with the initial upward leader and terminating with the long continuing current in the last stroke.

High-speed video observations are limited to resolving lightning evolution outside the thunderstorm cloud. To reconstruct the full morphology of the lightning flash, it is necessary to locate the electromagnetic radiation emitted during the discharge process. We used the LFM-LMS system to reconstruct the detailed 3D structure of the lightning flash (as shown in Figure 2). Each panel in Figure 2 shows the time-resolved mapping results from different perspectives. The flash started at 23:38:25.68 UTC; the upward leader induced lightning channels that propagated into two regions: branch A developed upward and then turned to the northwest of the triggering site; branch B circumambulated east before it propagated toward the cloud. Branch B mainly drained a charge region located southeast of the thundercloud. The major heights of the radiation sources located by the LFM-LMS varied from 4 to 7 km; the total length of the two main channels was about 15 km. We also compared the mapping results of Tr_201807 with the radar reflectivity of the parent thunderstorm (Figure 3), which shows the presence of two convection regions (with reflectivity >35 dBZ), one located to the northwest and the other to the south of the triggering site. At the time of Tr_201807, the thundercloud region over SHATLE exhibited low reflectivity and shallow depth; the lightning initiation point was located at

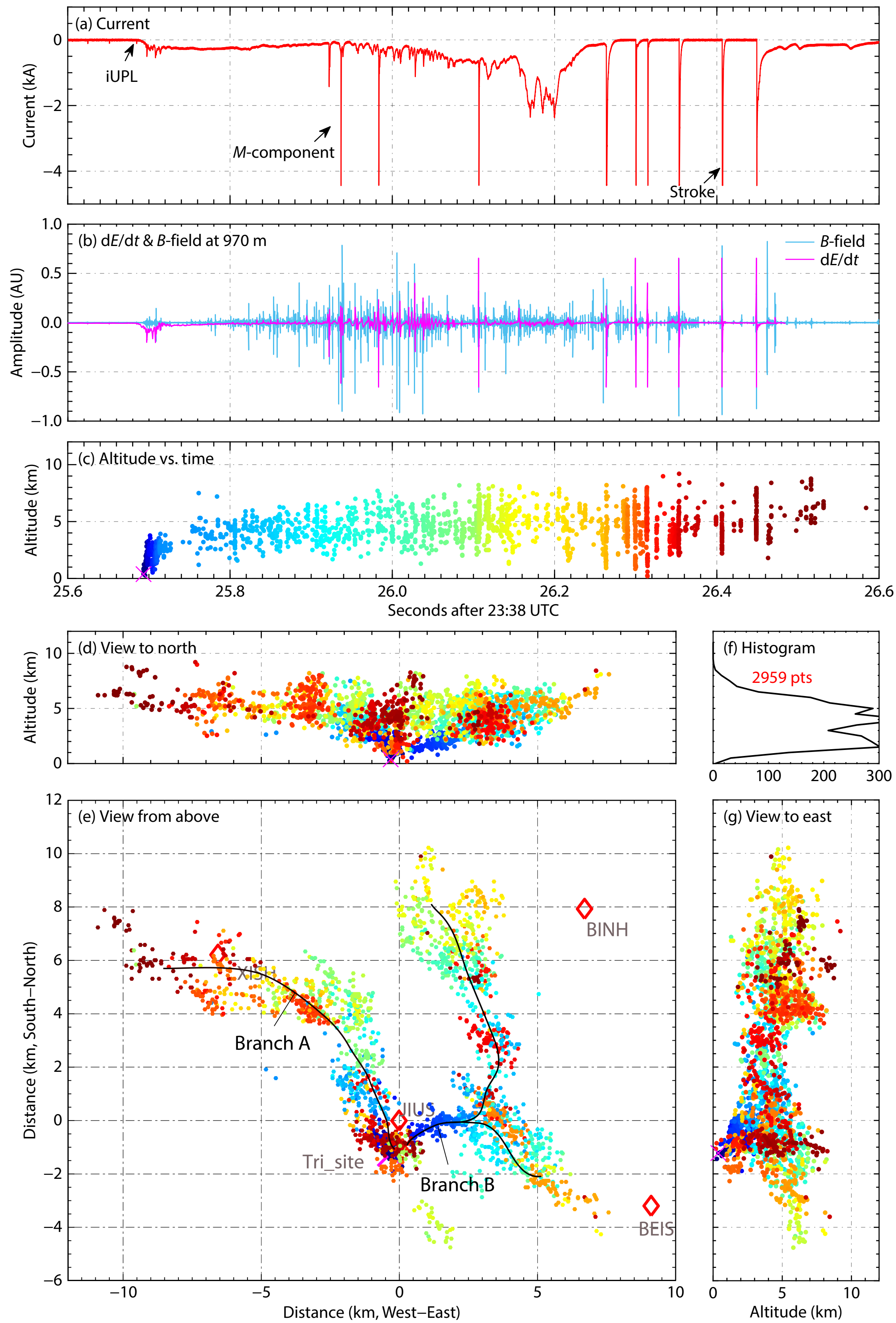

Figure 2. The d*E*/d*t* waveform (a) at 970 m, the vertically expanded current waveform (b), and 3D images of location results of triggered lightning Tr_201807; panels (c)–(g) show, respectively, the height-time view (with radiation sources located by the LFM-LMS color coded according to time), projection view to north, view from above, histogram of source height, and projection view to east. The red diamonds denote the sensor position. The purple cross indicates the first located source.

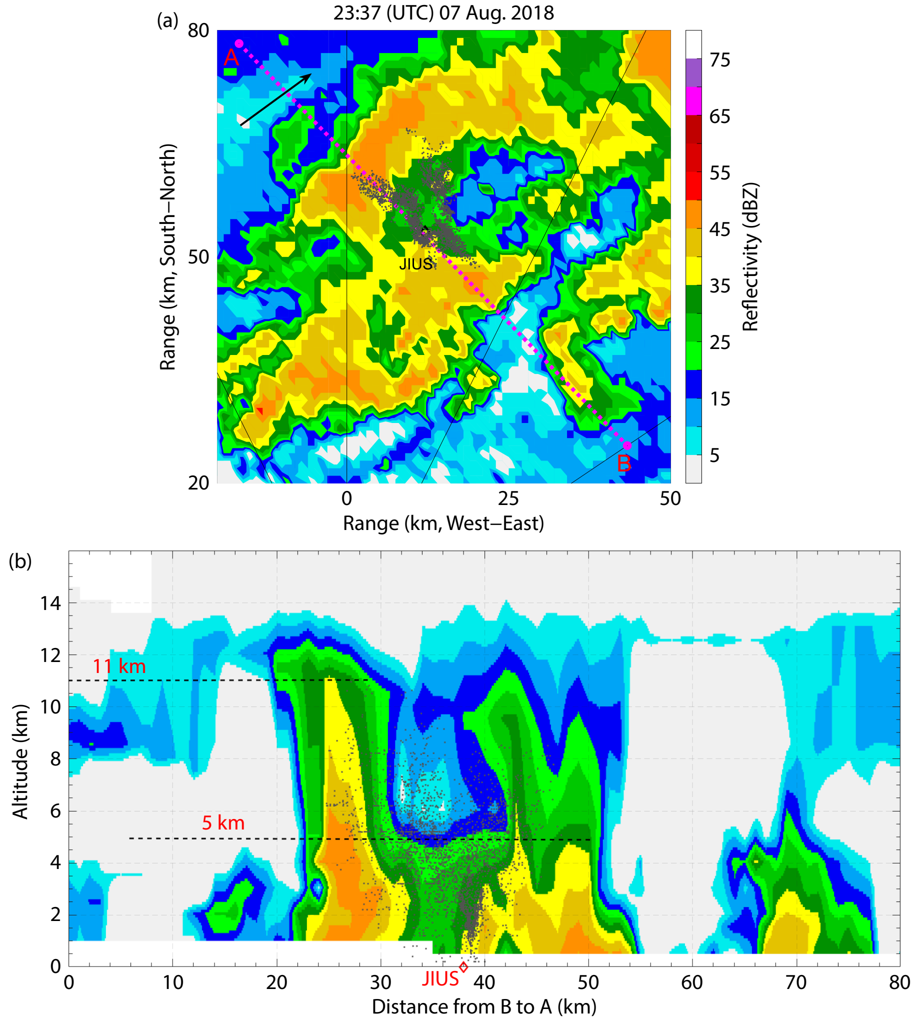

Figure 3. (a) Radar reflectivity overlapped with the lightning location sources (gray dots). (b) The vertical cross section of the radar echo along the pink dashed line AB in panel (a). The black arrow in panel (a) shows the moving direction of the thunderstorm. The red diamond denotes the position of triggering site.

the edge of the convective region to the southeast (Figures 3a and 3b).

3.1 Leader Propagation and Charge Transfer During the Initial Stage

After the rocket reached an altitude of 249 m above ground level (AGL), the initial upward positive leader (iUPL) emerged following several preliminary breakdown attempts (the high-speed camera did not capture this segment). The early stage of iUPL was composed of unipolar current pulses; the typical inter-pulse interval was approximately 25 μs (e.g., Lu GP et al., 2016a; Li X et al., 2021), and the pulse duration generally became wider while the upward positive leader ascended to higher altitude (e.g., Lu GP et al., 2016a; Fan YF et al., 2018). As shown in Figure 4a, over a period of 500 μs, the magnitude of the iUPL current pulses varied between −30 A and −100 A (a negative current pulse is defined as negative charge being transferred downward), with a total charge transfer of about −3.48 mC (mC = millCoulomb). The channel extended approximately 38 m, and its average two-dimensional (2D) propagation velocity (calculated from the 2D view), as determined by high-speed video analysis, was estimated to be about 7.7×10^4 m/s. About 2.4 ms after the iUPL onset, the upward propagating leader split at an altitude of about 370 m (marked in Figure 1a), into two leaders that then continued upward into different cloud regions and transferred negative charge to the ground. About 12 ms after the iUPL onset, a longer pulse related to branch A appeared with peak amplitude of −507 A, as did another pulse with peak of −547 A contributed by branch B. Within 36 ms, total charge transfer reached −6.48 C.

Abundant magnetic pulses were detected during the propagation stage of the aforementioned two upward positive leaders. Figure 4b displays the magnetic field measured at JIUS station, 970 m northeast of the triggering site, during this stage. As mapped by the LFM-LMS (see Figures 4c and 4d), branch A propagated upward to an altitude of 2 km and then turned northwestward, continuing its inclined upward propagation. Branch B, after exceeding an altitude of 1.0 km, extended northeastward and maintained its inclined ascent up to 3 km. From the LF magnetic waveform and the mapping results, it is obvious that the amplitude of the initial magnetic pulses in the BEW coil (i.e., the *B*-field

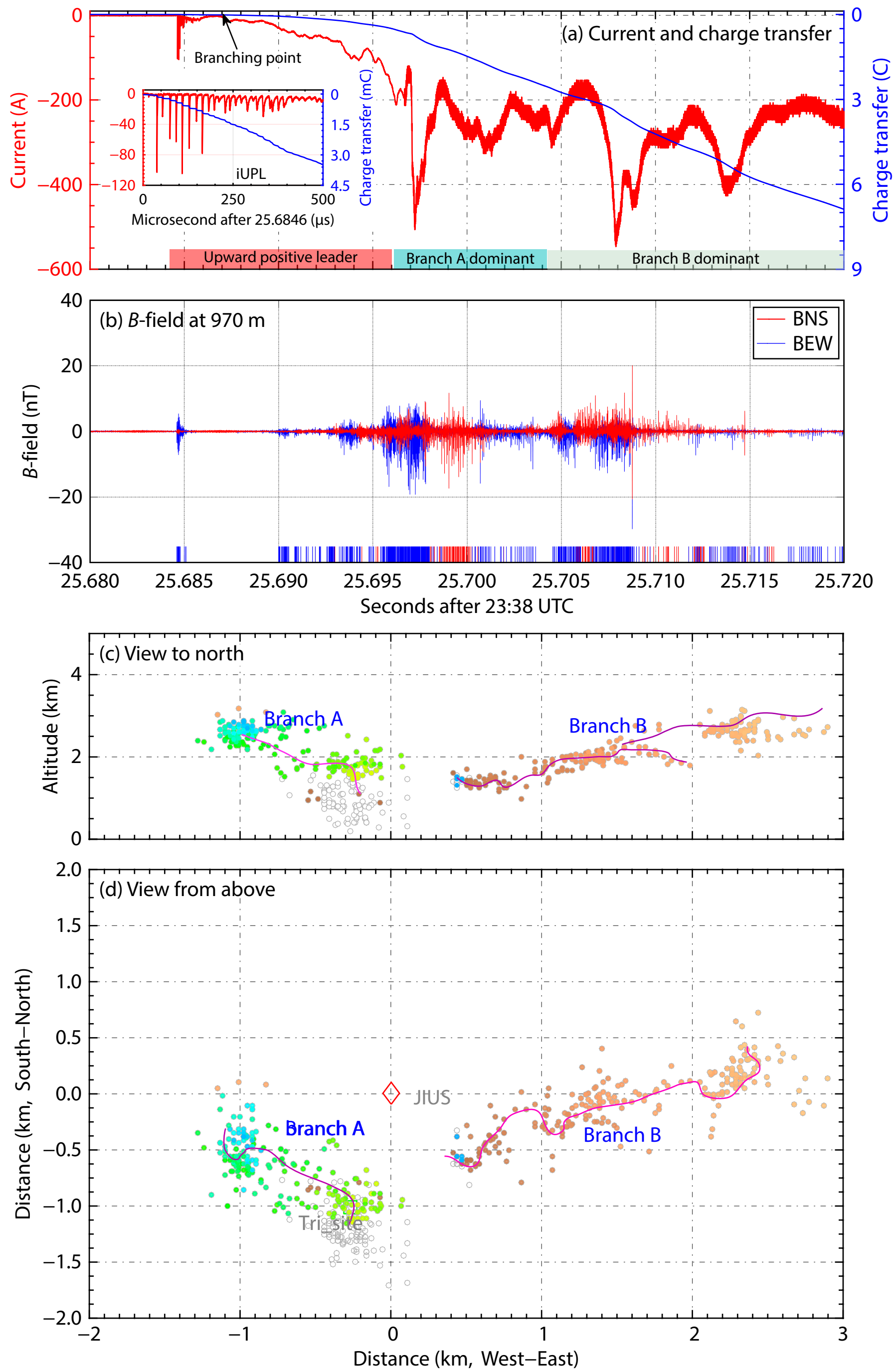

Figure 4. Channel-base current, charge transfer, associated magnetic field, and the radiation source location results based on LFM-LMS during the initial stage of upward leader propagation. (a) Channel-base current and accumulated charge transfer curve. (b) Magnetic field measured at 970 m away from the triggering site (note that BNS and BEW denote the signal in the north−south and the east−west direction, respectively). The red and blue short vertical bars in the figure indicate which magnetic pulse channel (BNS or BEW) is dominant at each corresponding time point. (c) The view north of source location results. (d) Birds-eye-view of the lightning channels. Gray circles denote radiation sources located outside the specified time period. Colored circles represent sources within the time period, with the color variation indicating temporal sequence: green corresponds to earlier times and brown to later times.

component in the east−west direction) was larger than that in the BNS coil (i.e., the north−south *B*-field component). The relative strengths of magnetic pulses in those two directions reversed when the upward leader propagated into the thundercloud. Specifically, when the BNS magnetic pulses exceeded that of BEW, the radiation originated predominantly from branch B propagating eastward; conversely, when the BEW magnetic pulses dominated, the radiation stemmed primarily from branch A. This observation suggests that the electromagnetic radiation from the impulsive charge transfer (due to negative breakdown) associated with a positive leader can be utilized to locate the leader tip (Stock et al., 2017). Also, we suggest that these observations support the conclusion that variation in the heading direction of lightning leaders causes the polarity reversal of observed magnetic pulses (e.g., Lu GP et al., 2014; Wang Z et al., 2023).

3.2 Charge Transfer by the Initial Continuing Current and Strokes

During this early stage, charge was transferred continuously to ground along the dual channels. It is inherently challenging to distinguish individual current contributions and transferred charge quantities from branch A and B, as both channels connected to the same main channel, and current measurements were taken at the channel base. However, high-speed video imagery in this case reveals a critical distinction: branch A exhibited discrete illumination–extinction cycles, with each illumination event synchronized precisely with current pulses, whereas branch B maintained continuous luminosity accompanied by steady charge transfer. This indicates that the current and charge transfer from branch A were superimposed on the continuous current of branch B. To quantify the charge transfer of branch A, the current preceding the leader connection of branch A (representing branch B's continuing current) is defined as the background current; the net charge transfer of branch A is then calculated by subtracting the integrated background current over the pulse duration from the integrated value of the measured current waveform.

The initial continuing current process persisted until branch A gradually decayed and extinguished, while branch B remained luminous. About –44 C negative charge was transferred to ground before the first downward negative leader (leading to *M*-component P#1 in Figure 5a) appeared in the camera's field-of-view.

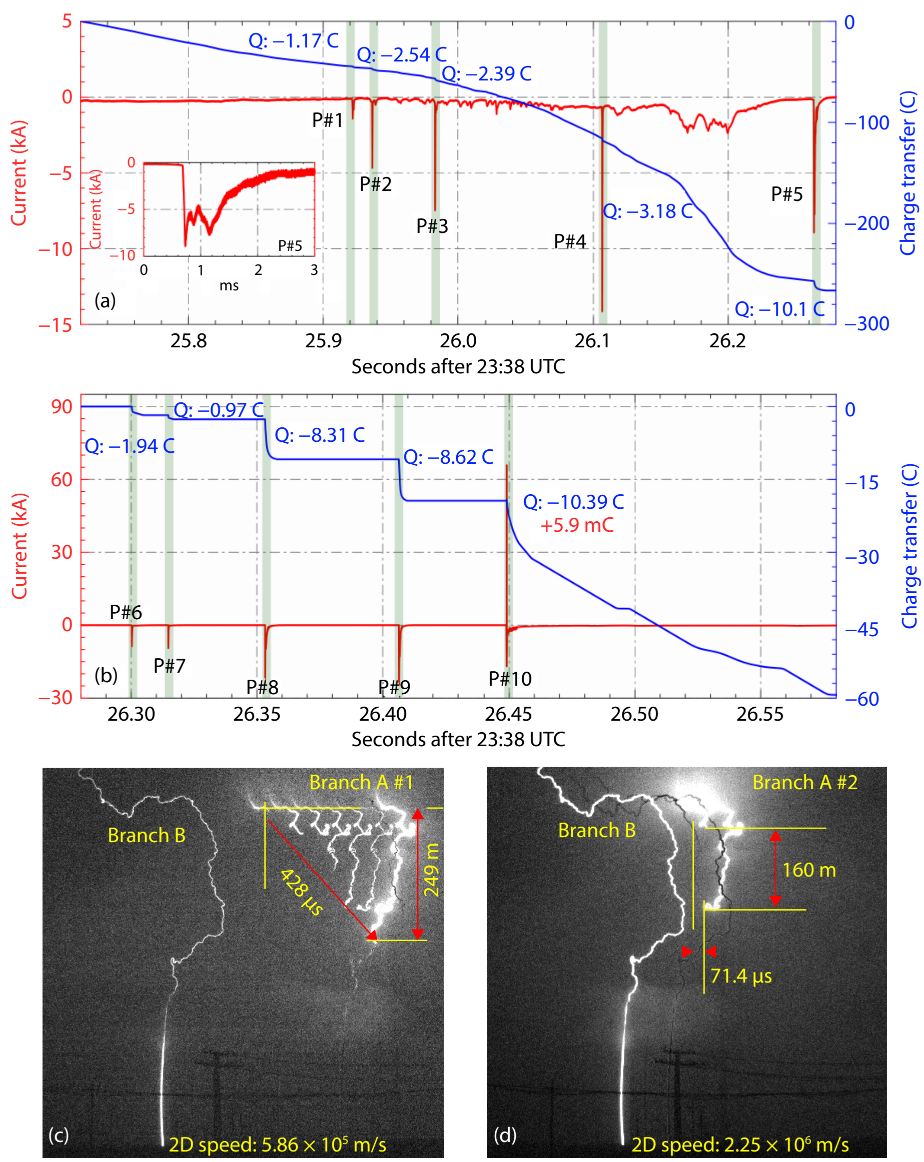

Figure 5. The current waveform and associated charge transfer during the stages of initial continuous current (a) and the subsequent strokes (b). (c) shows the downward channel extension of P#1 along branch A; (d) shows the downward channel extension of P#2 along branch A. P#1–5 are the *M*-component events; P#6–10 are CG strokes.

Within 428 μs, the downward leader descended 249 m in the vertical direction along branch A; the 2D extension speed of the downward leader is estimated to have been about 5.86 × 10^5 m/s. The lightning channel was suddenly illuminated when the downward leader connected to the main channel at the branching point. The current of the downward leader rose to a maximum of −1.41 kA at 119.4 μs; a total of −1.17 C negative charge was delivered during the time interval of 1.43 ms centered on the maximum current. Subsequently, branch A extinguished gradually, but branch B was still luminous with persistent charge transfer.

Branch A was first lit when a dart leader (causing *M*-component P#2) descended at a speed of 2.25 × 10^6 m/s and made connection with the branching point. The current increased to a peak of −4.53 kA within 12 μs; over 0.29 ms, −2.54 C negative charge was transferred to grounds. Three subsequent downward negative leaders caused *M*-components (referred to as P#3, P#4, and P#5, respectively) that exhibited peak strengths (charge transfers) of −7.5 kA (−2.39 C), −14.1 kA (−3.18 C), and −8.93 kA (−10.1 C), respectively (Figure 5a). Notably, *M*-component P#5 transferred significantly more charge to the ground than the others. The LFM-LMS mapping results show that the charge transfer related to P#1–5 was mainly from the northwest region of the cloud, at a height of 4–6 km and about 5 km from the triggering site. Combined with the radar echo, it can be seen that the lightning ignited in the convection zone with echo reflectivity >35 dBZ.

Branch B maintained its luminous state throughout this stage. Furthermore, numerous LF sources were present within the region of thundercloud with radar reflectivity <35 dBZ (Figure 3a). It can be deduced that the positive leader with higher potential intervened to the negative charge region and induced multiple breakdowns in the vicinity of the main channel. Therefore, negative charge rushed back to the main channel at a fast propagation speed to keep branch B luminous. After P#4 the magnitude of continuing current reached about −2 kA. Eventually, approximately −147 C negative charge was deposited to ground through branch B within 0.13 s, accounting for 44.1% of the total charge transfer (−333.32 C). The main charge transfer, according to the 3D mapping results, was from the thundercloud region that exhibited relatively weak reflectivity (<35 dBZ).

3.3 Source Positions and Charge Transfers of Subsequent Sstrokes

After 23:38:26.28 UTC, the channel-base current was nearly zero (see Figures 1b and 5b); although the channel luminosity of branch B was still faint, and the LF sources located by the LFM-LMS indicate that branch B also ceased to conduct at this stage. Therefore, the following dart leaders along branch A caused CG strokes rather than *M*-components.

The downward leader of P#6 caused the first subsequent stroke, with peak current of −8 kA and a slower rise edge (rise time was 37.7 μs) compared to the other strokes. Stroke P#7, however, exhibited features common to more typical CG strokes, identified in previous studies (Rakov, 1999; Schoene et al., 2009; Zheng D et al., 2013). Regarding the prolonged current rise times of P#6 and P#7, we propose the following mechanism: Although the main grounded channel cooled due to near-zero current (with consequent impedance increase), it maintained faint luminosity due to substantial residual charge. When P#6 and P#7 occurred, the newly injected charge underwent buffering and dispersion within the main channel, resulting in significantly extended rise times of the current waveform leading edges. CG strokes P#8 and P#9 carried higher peak current and were of longer duration, leading to more charge transfer (see Figure 5b and Table 1). Stroke P#10 contained an interesting and rarely observed current waveform, which peaked at −16.7 kA within 0.5 μs, then reversed its polarity to a positive peak of +65.73 kA over 0.8 μs, and returned to −15.1 kA within another 9.8 μs. Finally, the current gradually decayed into the form of a long-lasting continuing current.

According to the LFM-LMS mapping results, strokes P#6–9 were related to the charge transfer from altitudes of 5–8 km in the northwest cloud region of the triggering site. For stroke P#10, there were also some radiation sources in the northwest, but most

Table 1. Characteristics of current pulses passing along branch A.

No.	Peak current (kA)	Rising time (10%–90%, μs)	Duration (ms)	Charge transfer (C)	Vertical extending speed of downward leader (m/s)	Charge moment change (C·km)
P#1	−1.41	119.4	1.43	−1.17	0.59 × 10^6	−5.8
P#2	−4.53	11.6	0.29	−2.54	2.25 × 10^6	−15.2
P#3	−7.47	17.0	0.38	−2.4	6.53 × 10^6	−13.2
P#4	−14.13	12.2	0.50	−3.18	7.28 × 10^6	−15.9
P#5	−8.93	36.4	2.84	−10.1	1.62 × 10^6	−65.6
P#6	−8.8	37.7	0.38	−1.94	1.25 × 10^6	−13.2
P#7	−9.33	13.0	0.24	−0.97	1.60 × 10^6	−5.3
P#8	−23.73	2.9	1.68	−8.31	10.1 × 10^6	−58.2
P#9	−24.53	3.9	1.30	−8.62	NA	−60.3
P#10	−16.93/+65.73	0.5/1.3	3.03	−10.39 (−5.9 mC/+0.24 C/−10.14 C)	5.38 × 10^6	−72.2

Notes: "−" before the peak current denotes the current direction flowing upward. NA = Not available.

sources of P#10 were in the thundercloud at the height of 4–8 km above the triggering site, implying that the charge transfer related to P#10 was from a region in the thunderstorm different from those of P#9.

4. Discussion

4.1 Thunderstorm Convection and Lightning Process

According to 3D lightning mapping data and radar observations, the initiation point was situated precisely beneath the edge of the southeastern convective region (Figures 3a and 3b). As the upward positive leaders of branches A and B propagated into the cloud layer, they advanced preferentially toward regions exhibiting weaker radar echoes. Owing to the storm's dual convective cores, positioned northwest and south of the initiation point, branch A developed northwestward through a weak-convection zone before penetrating the >35 dBZ strong convection region, which was where the leaders of the five strokes P#6–10 started. Concurrently, branch B initially propagated vertically, then diverted eastward at ~500 m AGL, ascending along a tilted trajectory until it entered a weak-convection region at 3 km altitude characterized by subdued convective activity; then it extended northeastward to northward.

During the lightning process, ten downward negative dart leaders propagated along branch A, connecting to the grounded main channel, and triggered impulsive charge transfer. In contrast, branch B sustained prolonged ICC with persistent luminosity. This demonstrates that charged clouds within strong convection regions may more readily initiate charge transfer, but such charge transfer may be short-lived. That is why there were 10 negative dart leaders propagating downward along the previous channel, causing impulsive charge transfer when they reached the ground or the grounded main channel. The weak convection zone was a relatively extensive and stable cloud charge region, facilitating a continuous propagation of long-range electrical discharge (Bruning and MacGorman, 2013; Zhang ZX et al., 2017). Detection of abundant radiation sources indicates that the negative leader extended multiple branches into this area, and thus transferred a large amount of charge along the existing channel into the ground.

Among these ten pulses, P#1–5 correspond to *M*-components, while P#6–10 represent return strokes (see the complete conceptual diagram illustrated in Figure 6b). During the pulse process of

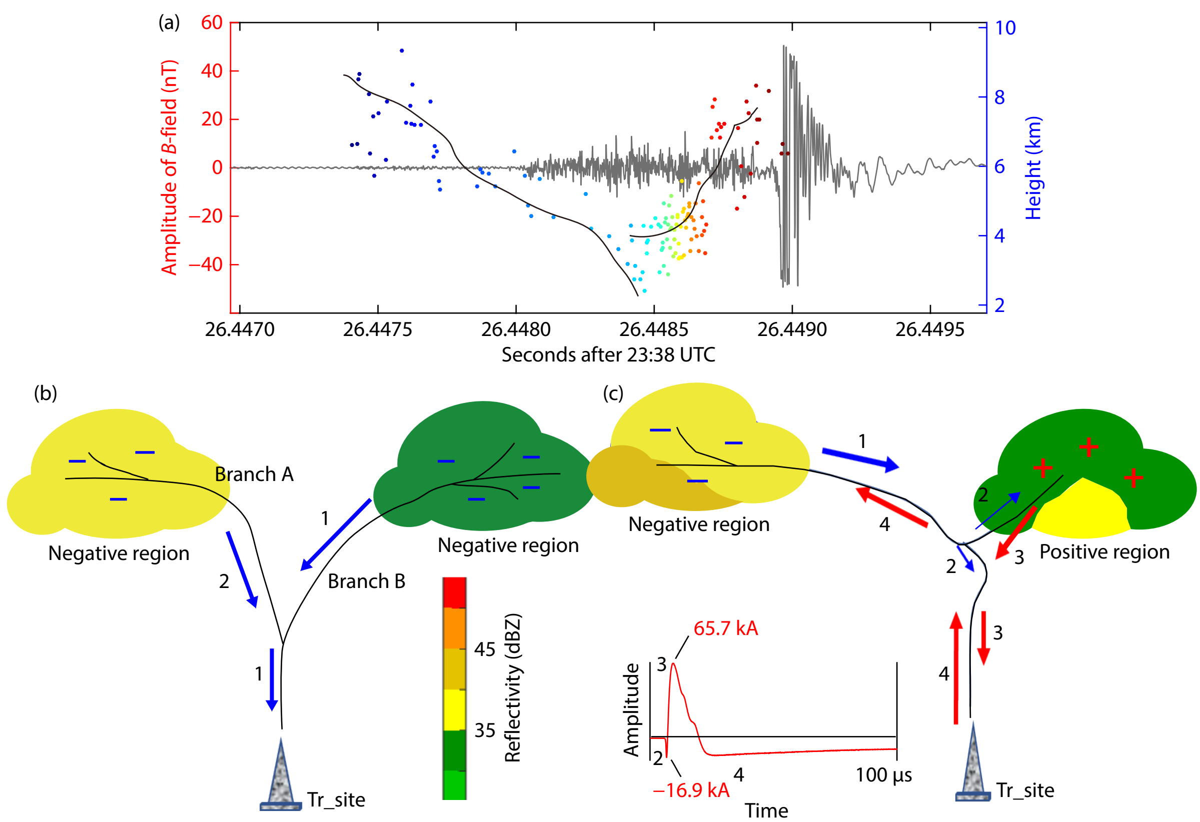

Figure 6. Mapping results (a) and schematic diagram (c) for the charge transfer of stroke P#10. At the first phase, the dart leader (marked by 1 in the diagram) from the negative charge region branched into two parts (marked by 2) at the altitude of about 2 km over the triggering site. One of negative leaders developed upward into the positive charge region; the other leader propagated down to the ground. At the second phase, positive charge transferred along the branching channel (established by the branched downward leader) (marked by 3). At last, the negative charge was transferred from a region dominated by negative charge (marked by 4). (b) illustrates the charge process in P#1–5: branch B continuously and steadily transferred negative charge to ground; concurrently, a negative dart leader initiated from the negative charge region tapped by branch A, connected to the main grounded channel, and transferred negative charge to ground. P#6–10 pertained exclusively to branch A and had no bearing on branch B.

P#1–5, the negative leader initiated within the negative charge cloud area where branch A was located. It propagated along the previous channel towards the starting point of the lightning, until it connected to the branch B which was continuously and stably transmitting negative charges to the ground, thereby causing a sudden increase in the current. Waveform analysis confirms that, during the P#6–10 pulse events, the initial continuing current phase had terminated. Branch B had ceased all charge transfer to ground; subsequent electromagnetic activity originated exclusively from processes within branch A. Throughout these processes, downward negative leaders consistently initiated within the strong convective area where branch A was located, and then subsequently propagated along the preconditioned channel toward ground, ultimately establishing return strokes upon contact.

4.2 Formation of Strong *M*-component

High-speed video observations clearly captured the dart/stepped leaders and their associated strong current pulse-enhanced luminosity features propagating through channel A during the ten sequential, intense discharge events. The first five pulses (P#1–5) are identified as *M*-components (Qie XS et al., 2011), which were followed by five subsequent CG strokes (Rakov, 1999; Zheng D et al., 2013). Therefore, the dart leader developed downward along branch A ten times, and the downward leaders with long in-cloud channel made connections with the active channel of branch B at the branching point (e.g., Zhang Y et al., 2018), resulting in *M*-components with intense current and larger charge transfer. In particular, *M*-component P#5 transferred approximately −10.1 C of negative charge to ground within 2.84 ms, exhibiting a rise time as long as 36.4 μs. This rise time was longer than that of the preceding *M*-components, with the exception of the first one (119.4 μs) (see Table 1). As shown in the inset of Figure 5a, a prominent protuberance was superposed on the falling edge after the main pulse of P#5; Qie XS et al. (2011) described such an event as a *Return stroke–M component* (RM) pulse because it exhibited the features of both *M*-component and CG strokes.

Prior to this, the cloud charge transfer associated with branch B was in a relatively stable state, with the maximum current exceeding −2 kA. Following the connection of the downward dart/stepped leaders of P#2–4 to the main grounded channel, the negative charge that they were transferring entered the main channel, which was already in a highly ionized state. This resulted in an alteration of the current pulse waveform's rising edge. Measurements at the channel base exhibit a slight delay, corresponding to the fact that the rise times of P#2–4 were slightly longer than 10 μs (as shown in Table 1). However, when the dart/stepped leader of P#5 propagated down (at 23:38:26.26 UTC) and connected to the main channel, which had become cool (and thus had enhanced impedance) due to small or negligible current flow, the new-arriving charges were dispersed and buffered in the main channel so that the front of the current waveform exhibited a relative long rise time.

Stroke P#6 also appeared at this stage; the rise time of its current pulse was longer than those of the following strokes. However, when the main channel extinguished after the first subsequent strokes, the following downward leaders in branch A (such as the leader in strokes P#8–10, as shown in Table 1) reignited the main channel and culminated in more strokes. The development of a downward leader in the main channel was the same as that in branch A, and as a result, the current wave front did not change and the rising edge of the current pulse measured at the channel base was still steep.

4.3 Possible Reason for the Current Polarity Reversal of Stroke P#10

From the channel-base current measurement, stroke P#10 as the last stroke exhibited a negative–positive–negative variation in the current polarity. It is crucial to elucidate the cause of this polarity reversal and the corresponding in-cloud progress of lightning leaders. Mapping results indicate that, during leader channel propagation, the stroke that occurred approximately 1 ms preceding this return stroke originated within the northwestern quadrant with reflectivity >35 dBZ (Figure 6a). The leader channel penetrated the weak echo region and propagated to an altitude approximately 2 km above the lightning initiation point. Radiation source localization within this region indicates that the lightning channel appears to have split and developed into two distinct branches: one continued to develop from the 2 km height upward to the height of 8 km, and the other one declined along the previous channel. Our mapping results did not show abundant radiation sources below 2 km for the downward leader. This could be attributed to the poor response of the LF sensor to the high frequency radiations of the dart leader, which advanced along the previous lightning path with relatively high conductivity.

Figure 6c shows a conceptual diagram for the charge transfer of this stroke based on the mapping results combined with our interpretation of surface *E*-field change. It is important to note that this process pertains exclusively to branch A and has no bearing on branch B. The negative leader was initiated within the high-reflectivity region in the northwest and then propagated along its channel toward the high-reflectivity core region within the thunderstorm area above the lightning initiation point. In this region, the negative leader bifurcated; one branch entered into a positive charge region, and the other went down to the ground. Therefore, part of the negative charge from the origin was deposited into the positive charge region and the rest was transferred along the channel (of branch A) to ground, causing a moderate CG stroke with peak current of −16.93 kA. Meanwhile, another negative leader extended into the positive charge region, establishing a fully ionized channel. This triggered a positive charge recoil (equivalent charge transfer) along branch A, resulting in reversal of current polarity and a peak current of +65.73 kA. However, due to the limited amount of positive charge and the dominance of the northwest negative charge region, not only was the positive charge in the channel neutralized, but also −10.14 C negative charge was transferred to ground.

5. Conclusions

This paper reports on a rocket-triggered lightning flash featuring a rare distinct branching in the initial upward positive leader. Based on high-speed video observation, channel-base current measurement, and low-frequency magnetic field and *E*-field change data, the charge transfer during this unusual lightning flash was examined in detail. We reconstructed the 3D channel structure of the triggered lightning, and quantified the charge transfer at each developmental stage. Specifically, we examined the propagation mechanisms and charge removal zones of several special discharge events. Our main conclusions are as follows:

The branched upward leaders progressed into different regions in the thunderstorm. The branch A leader induced ten successive dart leaders back to the ground, causing five *M*-components and five CG strokes with current peaks ranging from −1.4 to −25 kA and charge transfer of −0.9 C to −10.4 C. The branch B leader propagated into the northeast area, where the positive leaders progressed in an extensive charge region contoured by radar reflectivity <35 dBZ. Eventually, approximately −250 C negative charge was transferred to ground by branch B. This huge amount of charge transfer reflects an extensive distribution of negative charge in the thunderstorm.

The formation of *M*-components is associated with the connection between lightning leader and a pre-existing channel. A descending dart leader, propagating through elongated channels within thundercloud, triggered intense *M*-component events or strokes. Furthermore, the degree of ionization in the main channel directly modulated the rise time and duration of the current waveform.

We note that the polarity reversal of the current in the final return stroke resulted from branching of the downward negative leader, which is different from the case caused by the temporary termination of a negative leader as reported by Li X et al. (2021). Here, one of the branched negative leaders propagated downward to ground and the other one extended into the positive region to withdraw the positive charge downward. Eventually, the negative charge was transferred from the origination region with abundant negative charge.

The conclusions above supplement our understanding of rocket-triggered lightning—its origination, leader progression, channel elongation, and the observed current polarity reversal.

The triggered lightning examined in this work was not planned; it occurred by accident. The main conclusions are thus probably valid only for this specific case. Validation or modification of our conclusions will require study of additional similar cases, especially natural lightning cases. In addition, we acknowledge that our 3D mapping results are insufficient to depict the lightning morphology inside thunderclouds, because of the relatively low sampling rate (1 MHz) and contamination of the raw signal by background noise. Therefore, we suggest that the capability of the LMF-LMA should be upgraded in order to facilitate future studies. Moreover, since the charge transfer in natural lightning cannot be measured directly, as it can in triggered lightning, to achieve relatively accurate estimations of charge transfer during the IC and CG discharges we will need improved remote sensing techniques.

Data Availability Statement

All the data used for the analyses in this paper are available from https://zenodo.org/record/5554229#.Ya3j8dBByUl; further information is available upon request from Gaopeng Lu (gaopenglu@gmail.com).

Acknowledgments

This work was supported by National Key R&D Program of China (2023YFC3007703, 2017YFC1501501), the CAS Project of Stable Support for Youth Team in Basic Research Field (YSBR-018), National Natural Science Foundation of China (41875006, and U1938115), Youth Innovation Fund Project of the University (WK2080000172), the Chinese Meridian Project.

References

Bitzer, P. M., Christian, H. J., Stewart, M., Burchfield, J., Podgorny, S., Corredor, D., Hall, J., Kuznetsov, E., and Franklin, V. (2013). Characterization and applications of VLF/LF source locations from lightning using the Huntsville Alabama Marx Meter Array. *J. Geophys. Res.: Atmos.*, *118*(8), 3120–3138. https://doi.org/10.1002/jgrd.50271

Bruning, E. C., and MacGorman, D. R. (2013). Theory and observations of controls on lightning flash size spectra. *J. Atmos. Sci.*, *70*(12), 4012–4029. https://doi.org/10.1175/jas-d-12-0289.1

Cummer, S. A., and Lyons, W. A. (2004). Lightning charge moment changes in U. S. high plains thunderstorms. *Geophys. Res. Lett.*, *31*(5), L05114. https://doi.org/10.1029/2003GL019043

Edens, H. E., Eack, K. B., Eastvedt, E. M., Trueblood, J. J., Winn, W. P., Krehbiel, P. R., Aulich, G. D., Hunyady, S. J., Murray, W. C., … Thomas, R. J. (2012). VHF lightning mapping observations of a triggered lightning flash. *Geophys. Res. Lett.*, *39*(19), L19807. https://doi.org/10.1029/2012GL053666

Fan, Y. F., Lu, G. P., Jiang, R. B., Zhang, H. B., Li, X., Liu, M. Y., Qie, X., Zheng, D., Lyu, W., … Zhang, Y. J. (2018). Characteristics of electromagnetic signals during the initial stage of rocket-triggered lightning. *J. Geophys. Res.: Atmos.*, *123*(20), 11625–11636. https://doi.org/10.1029/2018JD028744

Fan, Y. F., Lu, G. P., Zhang, Y., Lyu, W., Zheng, D., Fan, X. P., Li, X., and Zhang, Y. J. (2020). Characterizing radio frequency magnetic radiation of initial upward leader stepping in triggered lightning with interferometric lightning mapping. *Geophys. Res. Lett.*, *47*(22), e2020GL089392. https://doi.org/10.1029/2020GL089392

Fisher, R. J., Schnetzer, G. H., Thottappillil, R., Rakov, V. A., Uman, M. A., and Goldberg, J. D. (1993). Parameters of triggered-lightning flashes in Florida and Alabama. *J. Geophys. Res.: Atmos.*, *98*(D12), 22887–22902. https://doi.org/10.1029/93JD02293

Jiang, R. B., Qie, X. S., Wang, C. X., and Yang, J. (2013). Propagating features of upward positive leaders in the initial stage of rocket-triggered lightning. *Atmos. Res., 129–130*, 90–96. https://doi.org/10.1016/j.atmosres.2012.09.005

Karunarathne, S., Marshall, T. C., Stolzenburg, M., Karunarathna, N., Vickers, L. E., Warner, T. A., and Orville, R. E. (2013). Locating initial breakdown pulses using electric field change network. *J. Geophys. Res.: Atmos.*, *118*(13), 7129–7141. https://doi.org/10.1002/jgrd.50441

Krehbiel, P. R., Brook, M., and McCrory, R. A. (1979). An analysis of the charge structure of lightning discharges to ground. *J. Geophys. Res.: Oceans*, *84*(C5), 2432–2456. https://doi.org/10.1029/JC084iC05p02432

Li, X., Lu, G. P., Fan, Y. F., Jiang, R. B., Zhang, H. B., Li, D. S., Liu, M. Y., Wang, Y. P., and Ren, H. (2019). Underground measurement of magnetic field pulses during the early stage of rocket-triggered lightning. *J. Geophys. Res.: Atmos.*, *124*(6), 3168–3179. https://doi.org/10.1029/2018JD029682

Li, X., Lu, G. P., Jiang, R. B., Zhang, H. B., Fan, Y. F., Shi, T., Qie, X. S., Zhang, Y., Ren, H., … Zhang, Y. J. (2021). On the transition from precursors to the initial upward positive leader in negative rocket-triggered lightning. *J. Geophys. Res.: Atmos.*, *126*(17), e2020JD033926. https://doi.org/10.1029/2020JD033926

Li, X., Lu, G. P., Lyu, F. C., Zhang, H. B., Qamar, K., and Jiang, R. B. (2023). Development of a low-frequency magnetic lightning mapping system (LFM-LMS) in North China: validation and preliminary results. *Earth Planet. Phys.*, *7*(4), 1–11. https://doi.org/10.26464/epp2023047

Lu, G. P., Cummer, S. A., Li, J. B., Han, F., Blakeslee, R. J., and Christian, H. J. (2009). Charge transfer and in-cloud structure of large-charge-moment positive lightning strokes in a mesoscale convective system. *Geophys. Res. Lett.*, *36*(15), L15805. https://doi.org/10.1029/2009GL038880

Lu, G. P., Winn, W. P., and Sonnenfeld, R. G. (2011). Charge transfer during intracloud lightning from a time-dependent multidipole model. *J. Geophys. Res.: Atmos.*, *116*(D3), D03209. https://doi.org/10.1029/2010JD014495

Lu, G. P., Cummer, S. A., Blakeslee, R. J., Weiss, S., and Beasley, W. H. (2012). Lightning morphology and impulse charge moment change of high peak current negative strokes. *J. Geophys. Res.: Atmos.*, *117*(D4), D04212. https://doi.org/10.1029/2011JD016890

Lu, G. P., Cummer, S. A., Li, J. B., Zigoneanu, L., Lyons, W. A., Stanley, M. A., Rison, W., Krehbiel, P. R., Edens, H. E., … Samaras, T. (2013). Coordinated observations of sprites and in-cloud lightning flash structure. *J. Geophys. Res.: Atmos.*, *118*(12), 6607–6632. https://doi.org/10.1002/jgrd.50459

Lu, G. P., Jiang, R. B., Qie, X. S., Zhang, H. B., Sun, Z. L., Liu, M. Y., Wang, Z. C., and Liu, K. (2014). Burst of intracloud current pulses during the initial continuous current in a rocket-triggered lightning flash. *Geophys. Res. Lett.*, *41*(24), 9174–9181. https://doi.org/10.1002/2014GL062127

Lu, G., Cummer, S. A., Tian, Y., Zhang, H. B., Lyu, F., Wang, T., Stanley, M. A., Yang, J., and Lyons, W. A. (2016a). Sprite produced by consecutive impulse charge transfers following a negative stroke: Observation and simulation. *J. Geophys. Res. Atmos.*, *121*(8), 4082–4092. https://doi.org/10.1002/2015JD024644

Lu, G. P., Zhang, H. B., Jiang, R. B., Fan, Y. F., Qie, X. S., Liu, M. Y., Sun, Z. L., Wang, Z. C., Tian, Y., and Liu, K. (2016b). Characterization of initial current pulses in negative rocket-triggered lightning with sensitive magnetic sensor. *Radio Science*, *50*(9). https://doi.org/10.1002/2016RS005945

Lyu, F., Cummer, S. A., Solanki, R., Weinert, J., McTague, L., Katko, A., Barrett, J., Zigoneanu, L., Xie, Y. B., and Wang, W. Q. (2014). A low-frequency near-field interferometric-TOA 3-D Lightning Mapping Array. *Geophys. Res. Lett.*, *41*(22), 7777–7784. https://doi.org/10.1002/2014GL061963

Lyu, F., Cummer, S. A., Lu, G. P., Zhou, X., and Weinert, J. (2016). Imaging lightning intracloud initial stepped leaders by low-frequency interferometric lightning mapping array. *Geophys. Res. Lett.*, *43*(10), 5516–5523. https://doi.org/10.1002/2016GL069267

Ma, Z. L., Jiang, R. B., Qie, X. S., Xing, H. Y., Liu, M. Y., Sun, Z. L., Qin, Z. L., Zhang, H. B., and Li, X. (2021). A low frequency 3D lightning mapping network in north China. *Atmospheric Research*, *249*, 105314. https://doi.org/10.1016/j.atmosres.2020.105314

Maggio, C. R., Marshall, T. C., and Stolzenburg, M. (2009). Estimations of charge transferred and energy released by lightning flashes. *J. Geophys. Res.: Atmos.*, *114*(D14), D14203. https://doi.org/10.1029/2008JD011506

Pasko, V. P., Inan, U. S., and Bell, T. F. (1997). Sprites as evidence of vertical gravity wave structures above mesoscale thunderstorms. *Geophys. Res. Lett.*, *24*(14), 1735–1738. https://doi.org/10.1029/97GL01607

Qie, X. S., Yang, J., Jiang, R. B., Wang, J. F., Liu, D. X., Wang, C. X., and Xuan, Y. J. (2010). A new-model rocket for artificially triggering lightning and its first triggering lightning experiment. *Chinese J. Atmos. Sci. (in Chinese)*, *34*(5), 937–946. https://doi.org/10.3878/j.issn.1006-9895.2010.05.09

Qie, X. S., Jiang, R. B., Wang, C. X., Yang, J., Wang, J. F., and Liu, D. X. (2011). Simultaneously measured current, luminosity, and electric field pulses in a rocket-triggered lightning flash. *J. Geophys. Res.: Atmos.*, *116*(D10), D10102. https://doi.org/10.1029/2010JD015331

Qie, X. S., Jiang, R. B., and Yang, J. (2014). Characteristics of current pulses in rocket-triggered lightning. *Atmos. Res.*, *135–136*, 322–329. https://doi.org/10.1016/j.atmosres.2012.11.012

Rakov, V. A. (1999). Lightning discharges triggered using rocket-and-wire techniques. *Recent Res. Dev. Geophys.*, *2*, 141–171.

Rakov, V. A., and Uman, M. A. (2003). *Lightning: Physics and Effects*. New York: Cambridge University Press.

Ren, H., Tian, Y., Lu, G. P., Zhang, Y. F., Fan, Y. F., Jiang, R. B., Liu, M. Y., Li, D. S., Li, X., and Qie, X. S. (2019). Examining the influence of current waveform on the lightning electromagnetic field at the altitude of halo formation. *J. Atmos. Sol. Terr. Phys.*, *189*, 114–122. https://doi.org/10.1016/j.jastp.2019.04.010

Ren, H., Lu, G. P., Cummer, S. A., Peng, K. M., Lyons, W. A., Liu, F. F., Li, X., Wang, Y. P., Zhang, S. B., and Cheng, Z. W. (2021). Comparison between high-speed video observation of sprites and broadband sferic measurements. *Geophys. Res. Lett.*, *48*(10), e2021GL093094. https://doi.org/10.1029/2021GL093094

Rison, W., Thomas, R. J., Krehbiel, P. R., Hamlin, T., and Harlin, J. (1999). A GPS-based three-dimensional lightning mapping system: Initial observations in central New Mexico. *Geophys. Res. Lett.*, *26*(23), 3573–3576. https://doi.org/10.1029/1999GL010856

Schoene, J., Uman, M. A., Rakov, V. A., Rambo, K. J., Jerauld, J., Mata, C. T., Mata, A. G., Jordan, D. M., Schnetzer, G. H. (2009). Characterization of return-stroke currents in rocket-triggered lightning. *J. Geophys. Res.: Atmos.*, *114*(D3), D03106. https://doi.org/10.1029/2008JD009873

Shi, D. D., Zheng, D., Zhang, Y., Zhang, Y. J., Huang, Z. G., Lu, W. T., Chen, S. D., and Yan, X. (2017). Low-frequency E-field Detection Array (LFEDA)-Construction and preliminary results. *Sci. China Earth Sci.*, *60*(10), 1896–1908. https://doi.org/10.1007/s11430-016-9093-9

Sonnenfeld, R. G., Battles, J. D., Lu, G. P., and Winn, W. P. (2006). Comparing *E* field changes aloft to lightning mapping data. *J. Geophys. Res.: Atmos.*, *111*(D20), D20209. https://doi.org/10.1029/2006JD007242

Stock, M. G., Krehbiel, P. R., Lapierre, J., Wu, T., Stanley, M. A., and Edens, H. E. (2017). Fast positive breakdown in lightning. *J. Geophys. Res.: Atmos.*, *122*(15), 8135–8152. https://doi.org/10.1002/2016JD025909

Thomas, R. J., Krehbiel, P. R., Rison, W., Hunyady, S. J., Winn, W. P., Hamlin, T., and Harlin, J. (2004). Accuracy of the lightning mapping array. *J. Geophys. Res.: Atmos.*, *109*(D14), D14207. https://doi.org/10.1029/2004JD004549

Wang, D., Rakov, V. A., Uman, M. A., Fernandez, M. I., Rambo, K. J., Schnetzer, G. H., and Fisher, R. J. (1999). Characterization of the initial stage of negative rocket-triggered lightning. *J. Geophys. Res.: Atmos.*, *104*(D4), 4213–4222. https://doi.org/10.1029/1998JD200087

Wang, Z. Y., Lu, G. P., Li, X., Zhang, H. B., Fan, Y. F., Ren, H., Zhang, C. X., Jiang, R. B., Qie, X. S., … Wang, Z. C. (2023). Low frequency magnetic field observations of natural positive leaders featuring stepwise propagation. *Geophys. Res. Lett.*, *50*(20), e2023GL105540. https://doi.org/10.1029/2023GL105540

Wu, T., Wang, D. H., and Takagi, N. (2018). Locating preliminary breakdown pulses in positive cloud-to-ground lightning. *J. Geophys. Res.: Atmos.*, *123*(15), 7989–7998. https://doi.org/10.1029/2018JD028716

Yoshida, S., Wu, T., Ushio, T., Kusunoki, K., and Nakamura, Y. (2014). Initial results of LF sensor network for lightning observation and characteristics of lightning emission in LF band. *J. Geophys. Res.: Atmos.*, *119*(21), 12034–12051. https://doi.org/10.1002/2014JD022065

Yuan, S. F., Qie, X., Jiang, R. B., Wang, D. F., Sun, Z. L., Srivastava, A., and Williams, E. (2020). Origin of an uncommon multiple-stroke positive cloud-to-ground lightning flash with different terminations. *J. Geophys. Res.: Atmos.*, *125*(15), e2019JD032098. https://doi.org/10.1029/2019JD032098

Zhang, Y., Zhang, Y. J., Zheng, D., and Lu, W. T. (2018). Characteristics and discharge processes of M events with large current in triggered lightning. *Radio Sci.*, *53*(8), 974–985. https://doi.org/10.1029/2018RS006552

Zhang, Z. X., Zheng, D., Zhang, Y. J., and Lu, G. P. (2017). Spatial-temporal characteristics of lightning flash size in a supercell storm. *Atmos. Res.*, *197*, 201–210. https://doi.org/10.1016/j.atmosres.2017.06.029

Zheng, D., Zhang, Y. J., Lu, W. T., Zhang, Y., Dong, W. S., Chen, S. D., and Dan, J. R. (2013). Characteristics of return stroke currents of classical and altitude triggered lightning in GCOELD in China. *Atmos. Res.*, *129–130*, 67–78. https://doi.org/10.1016/j.atmosres.2012.11.009